NASA CR-2001-210800

Ashitey Trebi-Ollennu, Terry Huntsberger, Yang Cheng,
E. T. Baumgartner, and Brett Kennedy

January 2001

In practice, uncertainty is generally structured because it is associated with specific model parameters or may be formulated in terms of norm-bounded perturbations of dominate and distinct elements within the system. Perturbations typically used to describe unstructured uncertainties are additive and multiplicative models. The multiplicative perturbation model is more useful than the additive perturbation model because it represents the uncertainty in a relative manner, rather than an absolute manner. Consider, for example, a multiplicative perturbation Δ_m bounded as follows, $\|\Delta_m\| \leq 0.3$. This implies the size of the perturbation does not exceed 30% of the nominal model. In the analysis to be presented in this section, only multiplicative perturbation models will be used.

In general, some ingenuity is usually required in selecting the dominant and distinct elements, or states, of a system to be used to formulate parameter uncertainty. This approach relies heavily upon the designer's knowledge and experience of what is technically feasible and practical. In the case of the Sun sensor, they are several candidates: the camera model, an estimate of 2-D Sun image centroid, Sun elevation, and the attitude (roll and pitch) of the rover. Uncertainties in the camera model parameters are beyond the scope of this paper. The interested reader is referred to (Y. Xiong 1997). Sensitivity analysis of the Sun sensor will focus on perturbation models for Sun centroid, Sun elevation, and rover attitude.

4.1.1 Impact of Sun Centroid Uncertainty on Sun Sensor Output

Section 3.2 presented the procedure for the estimation of a Sun image 2-D centroid and corresponding confidence. The complement of the confidence measure is, in effect, the degree of uncertainty in the 2-D centroid estimate.

4.1.1.1 2-D Centroid Position Dependent Error

To determine the error introduced by uncertainties in the estimated position of the 2-D centroid, the geometry of the imaging system comes into play. This geometry is shown in Figure 12, where f is the focal length of the lens and x is the offset from the center of the image plane. The error for determination of the angle φ is given by:

$$\delta\varphi = \frac{f}{\left(f^2 + x^2\right)}$$

The relative error/pixel decreases quadratically with distance from center of the image plane. The focal length for the lens is 2.5 mm; the width of the image plane is 8.4 mm. This geometry gives an error of 0.3 degrees/pixel in the center of the image, as shown in Figure 13, Figure 14, and Figure 15. These figures give alternate views of the angular error based on lens characteristics. The contour plot in Figure 14 illustrates that the error has decreased by 16% to 0.25 at 20 pixels away from the center of the image.

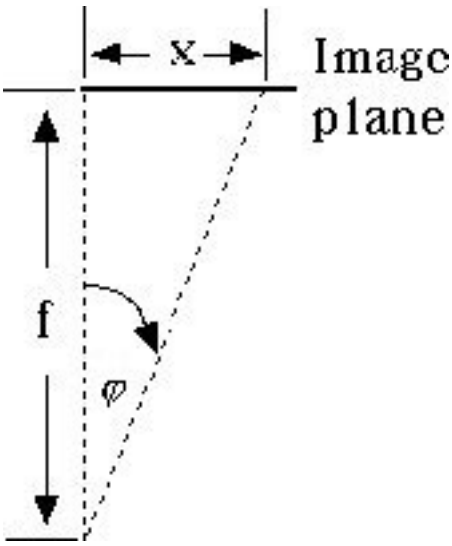
x
Image
plane
f
φ

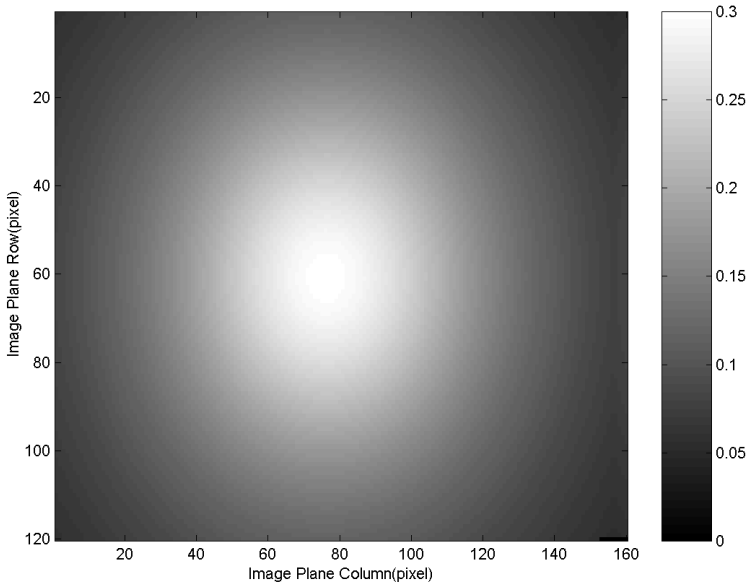
Image Plane Row(pixel)
Image Plane Column(pixel)
20
40
60
80
100
120
140
160
0.3
0.25
0.2
0.15
0.1
0.05
0

×

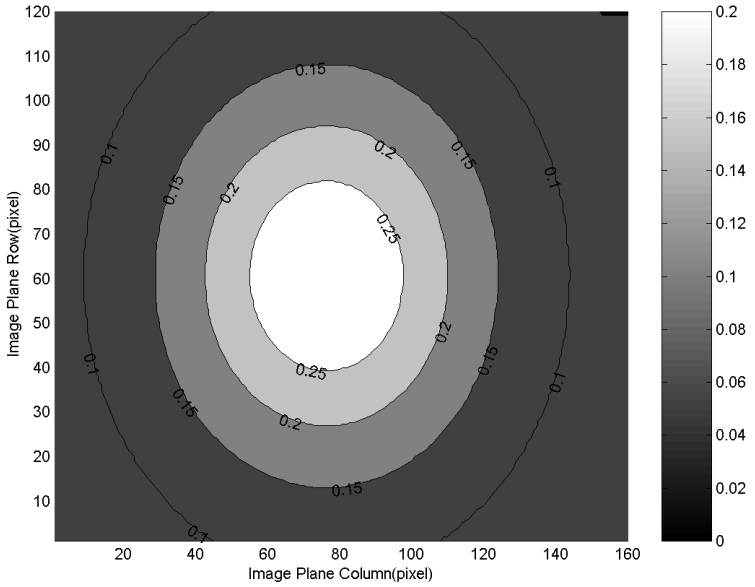
Image Plane Row(pixel)
Image Plane Column(pixel)
0.15
0.2
0.25
0.1

×

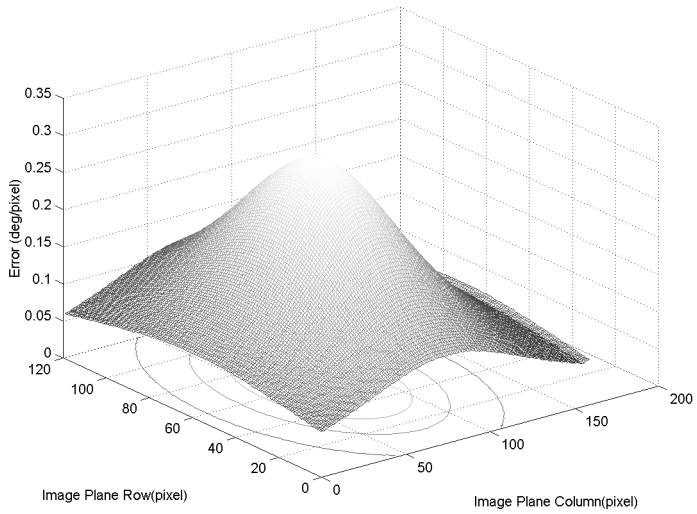
Error (deg/pixel)
Image Plane Row(pixel)
Image Plane Column(pixel)

×

Another error source is the heading error in the estimation of centroid of the Sun. This heading uncertainty ξ can be calculated as $\xi = \frac{s}{r}$, where s is the uncertainty in the centroid location and r is the distance from the center of the image. This measure is undefined at the exact center of the image; however, at 1 pixel away the measure is equal to 57.3° for a centroid uncertainty of 1 pixel. This is by far the main source of error in heading determination. The above analysis helped determined a cut-off region for centroid location in the image plane. A centroid located within a 20-pixel radius from the center of the image is discarded. In the cut-off region, an uncertainty of 1 pixel in the centroid will result in at least 2 degrees heading error; this is not acceptable.

4.1.2 Impact of Rover Attitude Uncertainty on Sun Sensor Output

As stated earlier, the FIDO rover is equipped with onboard an inertial navigation sensor (INS) to provide attitude information (roll and pitch) and attitude-rate information (roll rate, pitch rate, and heading rate). Uncertainty in the rover attitude may be a result of sensor imperfection, computational errors, and alignment errors. In addition, during rover traverse, the onboard INS may be subjected to nonlinear vibration; such motion arises as a result of rover wheels terrain interaction.

Let Δ_a be a block-diagonal matrix structure containing norm-bounded perturbations of the rover attitude roll and pitch, as follows:

$$\Delta_a = \begin{bmatrix} \delta_\phi & 0 \\ 0 & \delta_\theta \end{bmatrix} \text{and } \|\delta_\phi\| \le \vartheta_\phi \text{ and } \|\delta_\theta\| \le \vartheta_\theta$$

where δ_ϕ and δ_θ represents the multiplicative perturbations and ϑ_ϕ and ϑ_θ represent norm-bounds in the roll and pitch attitude of the rover, respectively. If the attitude of the rover is $A_r = [\phi, \theta]^T$, a multiplicative perturbation model for the rover attitude can be expressed as follows:

$$\delta_\phi \le \vartheta_\phi \phi \text{ and } \delta_\theta \le \vartheta_\theta \theta$$

Equation (21) represents a relative measure of the uncertainty in terms of the nominal value. Using equation (21) the rover attitude can now be expressed as follows,

$$A_r \le \begin{bmatrix} \phi(1+\vartheta_\phi) \\ \theta(1+\vartheta_\theta) \end{bmatrix}$$

Using equation (22), a complete sensitivity analysis of rover attitude uncertainties and its impact on the Sun sensor output can be investigated.

An experiment was setup on a cloudless day at JPL in Pasadena, California. The rover was positioned such that the Sun was within the field of view of the Sun sensor. The rover's attitude was as follows: roll = –0.906476 degrees and pitch = –15.446365 degrees. Using the Sun sensor, an image of the Sun was captured at 13 hours, 57 minutes, 27 seconds on 31 October 2000. The 2-D centroid of the Sun image was estimated to be $p_{row} = 181.197$ (pixels) and $p_{col} = 42.2379$ (pixels), with a confidence of 98.87%. Rover heading with respect to True North was determined to be 154.0154 (degrees). For the sensitivity analysis that follows, the above set of values for the centroid were assumed to the nominal values (99% confidence is close to ideal). To investigate the effect of rover roll uncertainty on the output of the Sun sensor, the norm-bound perturbations of rover roll and pitch were set as follows: $\vartheta_\phi = \pm 2.21$ and $\vartheta_\theta = 0.0$. Using equation (22) and the above values, the Sun sensor algorithm was run offline. The result is depicted in Figure 16. In the case of rover pitch uncertainty, the perturbation norm-bounds were set as follows: $\vartheta_\phi = 0.0$ and $\vartheta_\theta = \pm 0.13$. The results are shown in Figure 17.

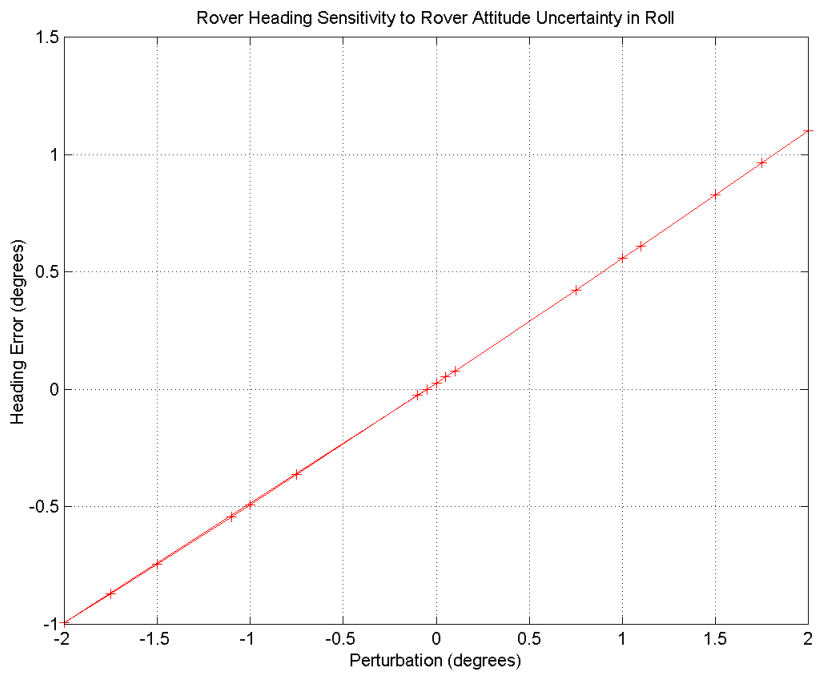

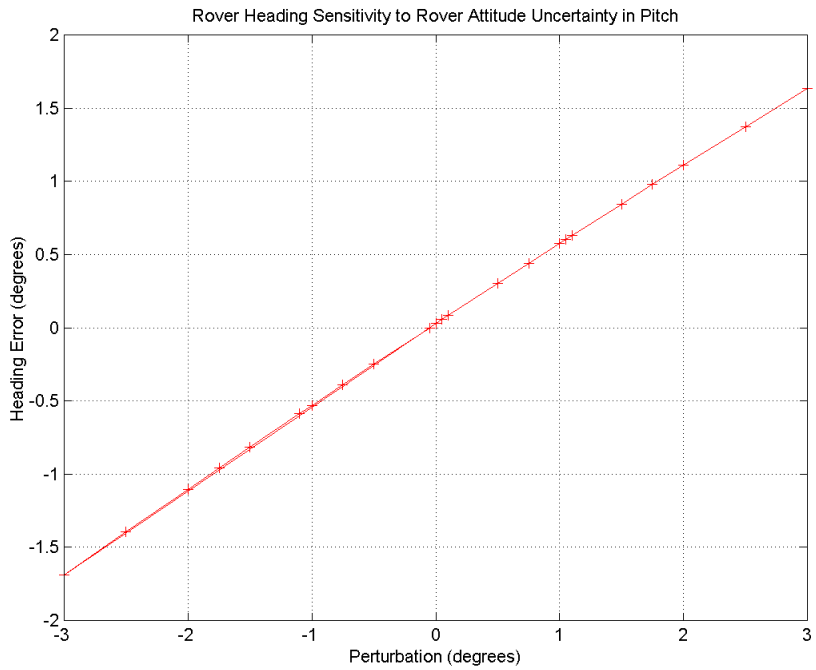

From Figure 16 and Figure 17 we observe that rover attitude uncertainty (in both roll and pitch) $< \pm 2^o$ have no significant effect on the Sun sensor output. However, uncertainties greater $\geq \pm 2^o$ can result in heading errors $\geq \pm 1^o$. In addition, we observe that the attitude uncertainty and its effect on heading error is a linear relation with a gradient of 0.5^o rover heading error per degree error in rover attitude. This suggest that if the rover attitude sensor is fairly robust, with a resolution less than a degree, the rover attitude will have no significant effect on the Sun sensor output. In addition to the above offline simulation, we setup an experiment to verify the above findings. The results are presented below.

The result of an experiment conducted with varying rover roll, but fixed rover pitch and heading angles, is presented in Table 1. The experiment covered half the operating envelope of the rover in roll (i.e., 0 to 32 degrees). The experiment results validated the simulation results. However, at 16 and 32 degrees roll there are significant heading errors ($\geq \pm 1^o$). This can be partially attributed to the low confidence Sun images (see Figure 20 and Figure 21). In addition, 2-D centroids are located in between regions 0.1 to 0.20 error/pixel (see Figure 14), compounding any errors. A complete set of Sun images for each roll angle is shown in Figure 18 to Figure 21.

In the same experimental setup, we varied the rover's pitch, with the rover roll and heading fixed. The results of this experiment are presented in Table 2; Sun images for each pitch angle are shown in Figure 22 to Figure 25. The heading errors as expected are less than a degree in line with the simulation results. However, a significant heading error ($\geq \pm 1^o$) is observed at pitch angle of 29 degrees. The non-circularity of the Sun disk (see Figure 25) introduces significant uncertainty in the estimate of the 2-D Sun centroid leading to significant heading error.

The experiments show that a gyroscopic bias of 0.01 degree/ sec would be more than suitable for the Sun sensor because the operation times for planetary rovers are typically of the order of a few hours. The result obtained from these experiments demonstrates that the Sun sensor is robust to rover attitude changes. This attribute will be very useful in rover exploration of valleys and impact craters of the Southern Hemisphere of Mars, where recent sitings suggest that liquid water has seeped out of surface gullies and alluvial fans. In such an environment, incremental odometry heading estimation of a rover is not suitable because the rover wheels would slip often due to the ruggedness of the terrain, leading to huge heading errors.

Rover Roll (degrees)	Time	2-D Centroid Row (pixels)	2-D Centroid Column(pixels)	Confidence (%)	Rover Heading (degrees)	Heading Error (degrees)
-0.70188	9:59 am	223.1341	27.73171	99.0	64.47	0.23
7.719	10:02 am	228.8544	71.55131	97.1	65.13	-0.43
15.7546	10:04 am	233.3887	113.0578	97.6	65.71	-1.01
31.94616	10:12 am	254.0006	202.6265	89.60	62.86	-1.84

Rover Pitch (degrees)	Time	2-D Centroid Row (pixels)	2-D Centroid Column(pixels)	Confidence (%)	Rover Heading (degrees)	Heading Error (degrees)
-0.23658	10:19 am	260.9356	36.10508	99.6	62.64	-0.64
5.899646	10:21 am	244.1236	36.82397	99.3	62.01	-0.01
14.98702	10:23 am	218.1802	37.82332	98.4	61.11	0.89
28.9010	10:25 am	175.1954	35.30651	98.1	60.07	1.93

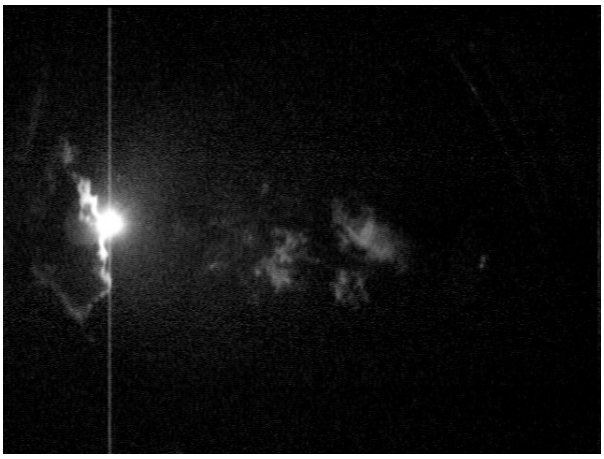

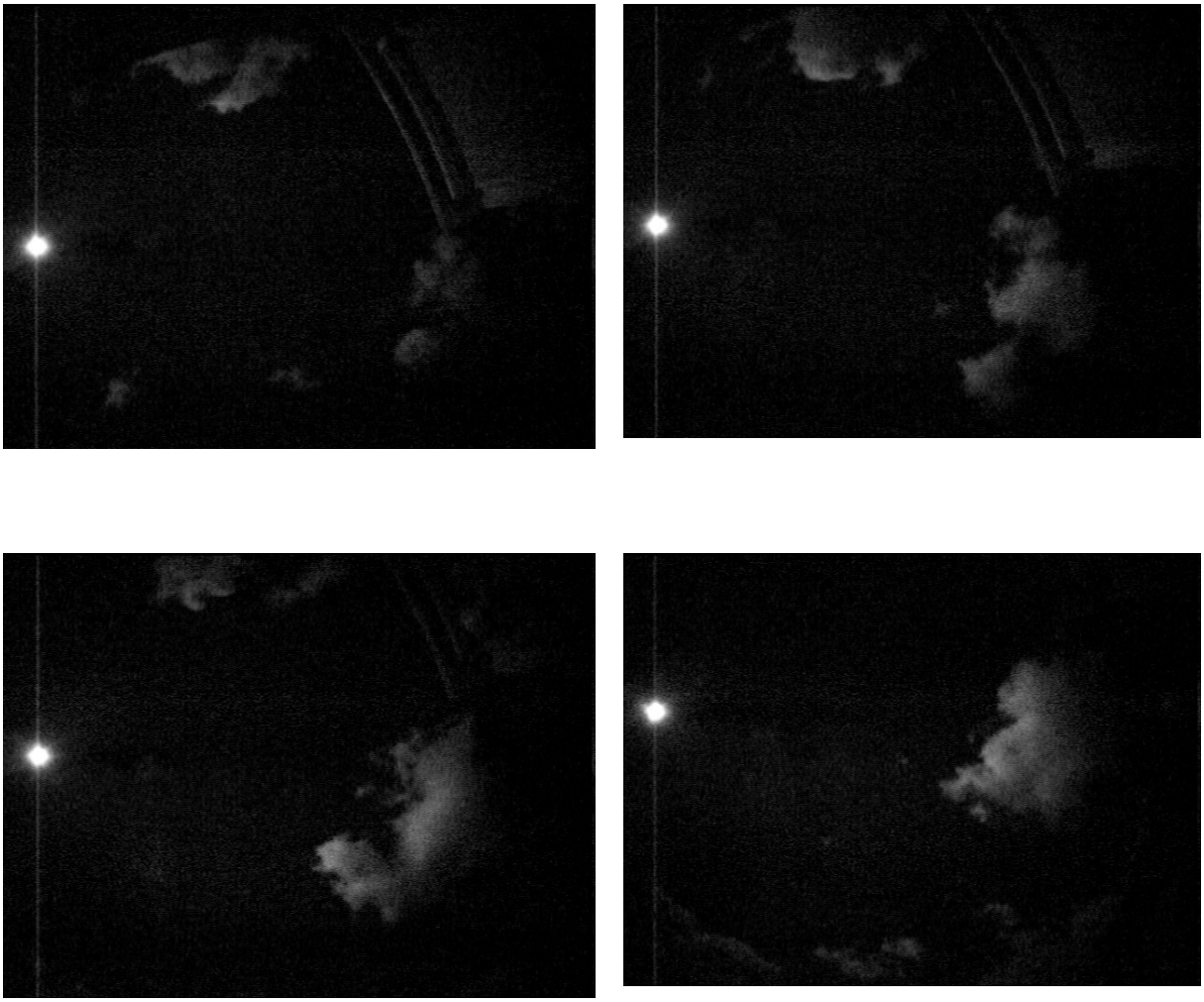

4.1.3 Impact of the Sun's Elevation on Sun Sensor Output

The Earth travels around the Sun in a circular orbit, with a different tilt angle from the Sun at different times of the year. This causes seasonal changes on Earth. For example, the summer Sun is at a higher elevation in the sky than the winter Sun. In addition, in the early morning or late afternoon (Sunrise or Sunset) the Sun is low in the sky in both the summer and winter. Typically, the Sun is at an angle that is most nearly vertical near solar noon.

In this section, we will investigate the sensitivity of the Sun sensor output with respect to the Sun's elevation over a 4-hour period (a typical operational period for a planetary rover). The Sun sensor FOV is rather restrictive; hence, the Sun is within the sensor FOV from about 10:00 am to 2:00 pm in the winter. This is only achieved after judicious positioning of the rover. On 31 October 2000 at 10:12 am, the rover was position with attitude, roll = –0.906476 degrees and pitch = –15.446365 degrees such that the Sun was within the view of the Sun sensor. At intervals of 5 minutes, a Sun sensor reading of the rover heading was collected until 1: 57 pm (approximately a 4-hour period). The day was cloudless, effectively eliminating or reducing the influence of atmospheric uncertainties as major factor in the Sun sensor output. The average confidence measure for the Sun images was 97%, confirming a cloudless day. Figure 26 depicts a plot of the Sun's azimuth against elevation for the duration of the experiment. The Sun's elevation and azimuth were obtained from ephemeris data and equation of time. Figure 27 depicts the trace of the 2-D location (centroid) of the Sun in images captured for the duration of the experiment. In contrast to Figure 26, Figure 27 is almost a straight line; the reason for this is that the Sun is at infinity with respect to the Sun sensor. Consequently, the radius of curvature is infinity; hence, the straight line. Also, the 2-D Sun centroid is moving across the image plane from left to right (see Figure 27).

Figure 28 shows the rover heading error against time, which can be interpreted as a plot of rover heading error against Sun elevation. In Figure 28, the heading error follows a quadratic profile with respect to the Sun's elevation. There are two main reasons for this trend. The first reason is that the Sun is moving across the image plane from a region of least error/pixel through the region with the worst error/pixel to a region of least error/pixel (see Figure 14) as discussed in section 4.1.1.1. The second reason is that as the Sun elevation rises the Sun captured in the image is relative large and non-circular (compared to low elevation Sun images). Similarly, at extremely low elevations, the Sun disk is very small and non-circular. The non-circularity and enlarge/very small image of the Sun introduces significant uncertainty in the 2-D Sun centroid estimate, leading to relatively large errors at Sunrise, solar noon, and Sunset. In Figure 28, the Sunrise period corresponds to 10:00 am to 10:30 am; the solar noon period corresponds to 11.45 am to 12.30 pm. Another source of error is the parametric uncertainty in the camera model with respect to the radial distortion of the wide FOV lens. The maximum heading error that occurs about noon is less than a degree. It is safe to conclude that the elevation of the Sun has no significantly impact on the output of the Sun sensor. The results obtained from the experiments would be used to formulate a new bias term in equation (18) to account for elevation of the Sun and the location of the 2-D Sun centroid in the image plane to further reduce the heading error.

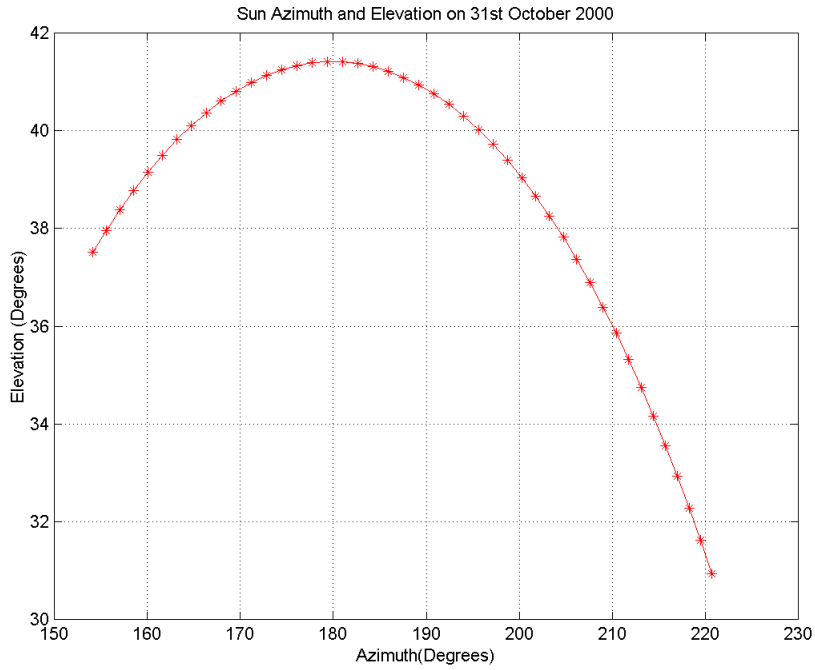
Sun Azimuth and Elevation on 31st October 2000
Elevation (Degrees)
Azimuth(Degrees)
42
40
38
36
34
32
30
150
160
170
180
190
200
210
220
230

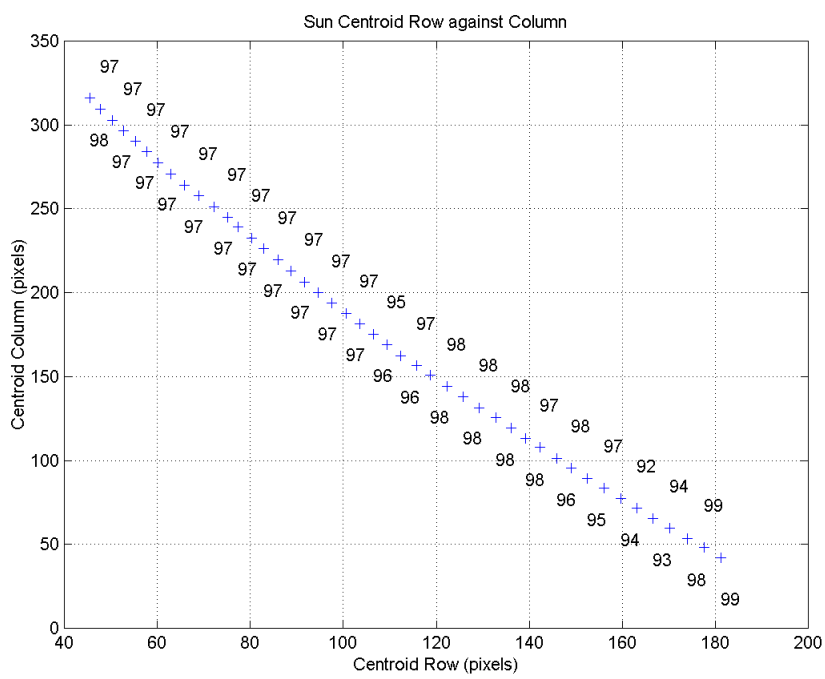
Sun Centroid Row against Column
Centroid Column (pixels)
Centroid Row (pixels)
350
300
250
200
150
100
50
0
40
60
80
100
120
140
160
180
200

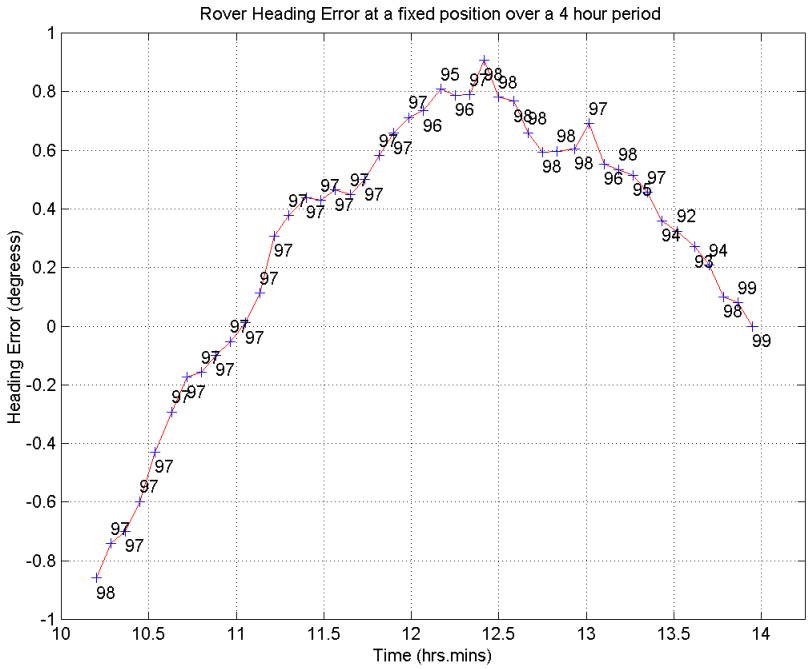

Figure 29 and Figure 30 depict the results of the above experiment conducted a day earlier (October 30, 2000) on a very cloudy day. These results are presented here to demonstrate the robustness of the Sun sensor to certain atmospheric conditions (e.g., clouds) and some limitations of the current Sun algorithm. Figure 29 depicts the trace of the 2-D location (centroid) of the Sun for the duration of the experiment. The average Sun image confidence for the experiment was 82%. Comparing Figure 29 to Figure 27 we observe significant point scatter (the effect of cloud cover). Nevertheless, the point scatter of 2-D Sun location in Figure 29 can be approximated with a straight line. This demonstrates the robustness of the 2-D Sun image centroiding to some atmospheric conditions. Figure 30 further demonstrates the robustness of the Sun sensor algorithm; under varying cloud cover, the heading errors are still within 1 degree (although there is a great deal more fluctuation in the heading error compared to Figure 28, as would be expected). Figure 31 and Figure 32 depict the best Sun images for the day with confidence of about 99%. On the other hand, Figure 33 to Figure 38 depict the five worst Sun images for the day. In Figure 35, it is virtually impossible for the human eye to see the Sun; however, the algorithm was able to detect the Sun location, resulting in the worse heading error, 0.9 degrees, a remarkable fit. In addition, the experiment helped determine the cutoff confidence for a good Sun image, which is $\geq 80\%$.

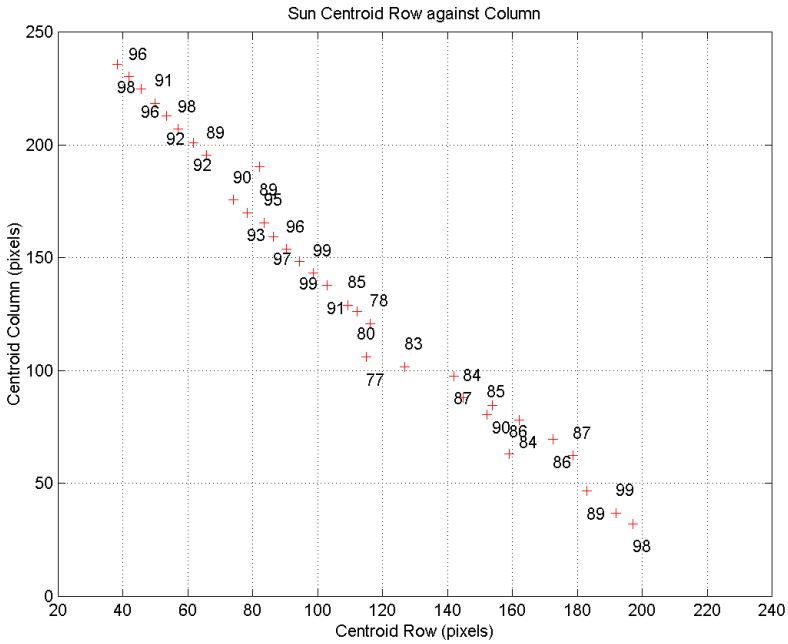
Sun Centroid Row against Column
Centroid Column (pixels)
Centroid Row (pixels)

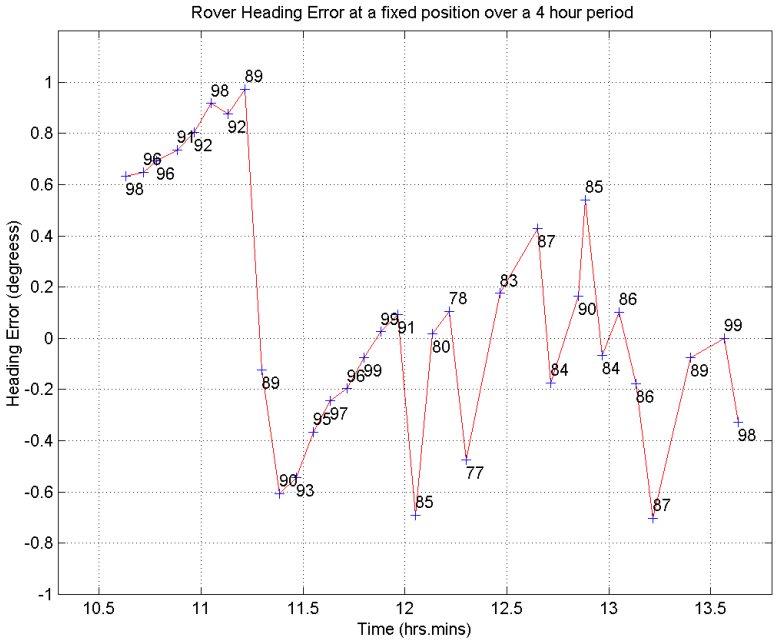
Rover Heading Error at a fixed position over a 4 hour period
Heading Error (degreess)
Time (hrs.mins)

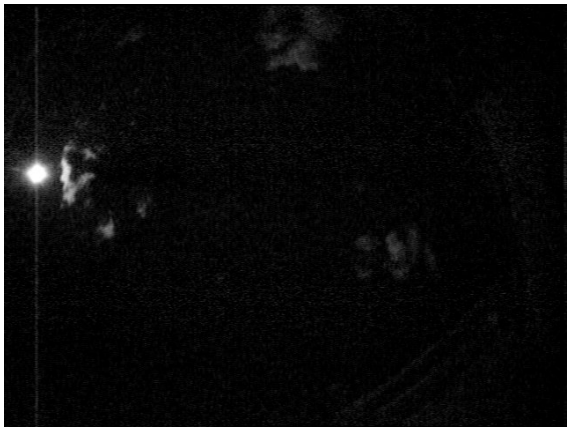

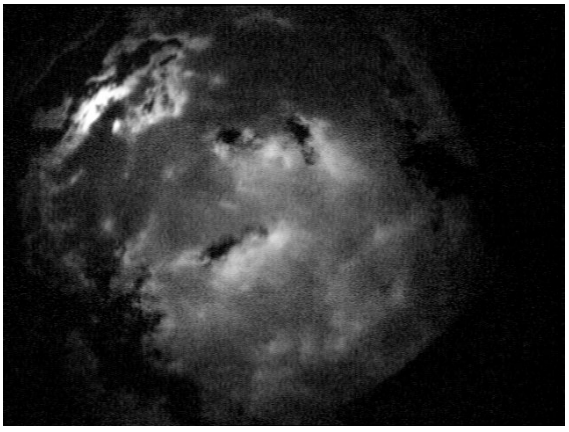

In this paper, we have presented extensive analysis, simulation, and experimental results of a new planetary rover Sun sensor for rover absolute heading detection. The new sensor can handle the effect of atmospheric conditions (cloud cover), changes in the Sun's position, and uncertainty in rover attitude measurements. The research reported here has led to a Sun sensor being included in the sensor suite for the NASA 2003 Mars rovers. One of the key uses for the Sun sensor on the 2003 mission will be to help point the high gain antenna on the rover to Earth and thereby establish communication at the end of a Sol.

A major disadvantage of the current design is the limited field of view of the lens. Research is currently on the way to develop a 150×150 FOV Sun sensor. Another major challenge is the collection of dust on the Sun sensor; this would be a major challenge for a 90-Sol mission, as planned for 2003. In addition, we are investigating the possible use of the Sun sensor to estimate the rover position during a very long traverse (e.g., $\geq 10 Km$) by employing concepts of solar point or geographic position (GP) of a body on a planet and circles of equal latitude.

1. Aleksandr Brandt, and, John F. Gardner (1998). Constrained Navigation Algorithms for Strapdown Inertial Navigation Systems with Reduced Set of Sensors. American Control Conference, Philadelphia, Pennsylvania.

2. Baumgartner, E. T. (2000). In-Situ Exploration of Mars Using Rover Systems. AIAA Space 2000 Conference, Long Beach, CA, AIAA.

3. D. H. Titterton, and, J. L. Weston (1997). Strapdown inertial navigation technology. London, Peter Pergrinus Ltd.

4. Doraiswami, R., and R. Stephen Price (1998). “A Robust Position Estimation Scheme Using Sun Sensor.” IEEE Transaction on Instrumentation and Measurement (2): 595-603.

5. E. T. Baumgartner, Hrand Aghazarian, A. Trebi-Ollennu, T. L. Huntsberger, and, M. S. Garrett (2000). State Estimation and Vehicle Localization for the FIDO Rover. Sensor Fusion and Decentralized Control in Autonomous Robotic Systems III, SPIE, Boston, MA, SPIE.

6. Gennery, D. B. (0000). Least-Squares Camera Clibration Including Lens Distortion and Automatic Editing of Calibration Points. To appear in "Calibration and Orientation of Cameras in Computer Vision". A. G. a. T. Huang, Springer-Verlag.

7. Levine, M. D. (1985). Vision in Man and Machine. New York, McGraw-Hill.

8. Moshier, S. L. (1987). Self-contained ephemeris calculator, Astronomy and numerical software source codes website, http://people.ne.mediaone.net/moshier/index.html. .

9. Nebot, E., and, Durrant-Whyte, H. (1997). Initial calibration and alignment of an inertial navigation. Fourth Annual Conference on Mechatronics and Machine Vision in Practice.

10. Paul G. Backes, and, Jeffrey S. Norris (2000). Mars Rover Mission Distributed Operations. TMOD Technology and Science Program News.

11. R. E. Arvidson, S. Squyres., E. T. Baumgartner, L. Dorsky, and, P. Schenker (2000). “Rover Trials for Mars Sample Return Mission Prove Successful.” EOS Transactions, American Geophysical Union (7): 65-72.

12. R.M. Haralick, S. R. Sternberg., and, X. Zhuang (1987). “Image analysis using mathematical morphology.” IEEE Trans. PAMI (4): 532-550.

13. Randel Lindemann, Lisa Reid, and, Chris Voorhees (1999). Mobility Sub-System for the Exploration Technology Rover. 33rd Aerospace Mechanisms Symposium.

14. Volpe, R. (1999). Mars Rover Navigation Results Using Sun Sensor Heading Determination. 1999 IEEE/RSJ International Conference on Intelligent Robot and Systems.

15. Wertz, J. R. (1995). Spacecraft Attitude Determination and Control, Kluwer Academic Publishers.

16. Y. Xiong, and, K. Turkowski (1997). Creating image-based VR using self-calibrating fisheye lens. IEEE conference on Computer Vision and Pattern Recongnition.

REPORT DOCUMENTATION PAGE

Form Approved
OMB No. 0704-0188

Public reporting burden for this collection of information is estimated to average 1 hour per response, including the time for reviewing instructions, searching existing data sources, gathering and maintaining the data needed, and completing and reviewing the collection of information. Send comments regarding this burden estimate or any other aspect of this collection of information, including suggestions for reducing this burden, to Washington Headquarters Services, Directorate for Information Operations and Reports, 1215 Jefferson Davis Highway, Suite 1204, Arlington, VA 22202-4302, and to the Office of Management and Budget, Paperwork Reduction Project (0704-0188), Washington, DC 20503.

1. AGENCY USE ONLY (*Leave blank*)

2. REPORT DATE
January 26, 2001

3. REPORT TYPE AND DATES COVERED
Final

4. TITLE AND SUBTITLE
Design and Analysis of a Sun Sensor for Planetary Rover Absolute Heading Detection

5. FUNDING NUMBERS
TA 100097 RMSA.R.A

6. AUTHOR(S)
Ashitey Trebi-Ollennu, Terry Huntsberger, Yang Cheng,
E. T. Baumgartner, and Brett Kennedy

7. PERFORMING ORGANIZATION NAME(S) AND ADDRESS(ES)
Jet Propulsion Laboratory,
California Institute of Technology
4800 Oak Grove Drive, Pasadena, California 91109

8. PERFORMING ORGANIZATION REPORT NUMBER
NASA-CR-2001-210800

9. SPONSORING/MONITORING AGENCY NAME(S) AND ADDRESS(ES)
National Aeronautics and Space Administration
Washington, DC 20546-0001

10. SPONSORING/MONITORING AGENCY REPORT NUMBER
NASA-CR-2001-210800

11. SUPPLEMENTARY NOTES

12a. DISTRIBUTION/AVAILABILITY STATEMENT
Subject Category: 19 Distribution: Standard
Availability: NASA CASI (301) 621-0390

12b. DISTRIBUTION CODE

13. ABSTRACT *(Maximum 200 words)*

This paper describes a new Sun sensor for absolute heading detection developed for the Field Integrated, Design and Operations (FIDO) rover. The FIDO rover is an advanced technology rover that is a terrestrial prototype of the rovers NASA/Jet Propulsion Laboratory (JPL) plans to send to Mars in 2003. The need for a Sun-sensor on planetary rovers lies in the fact that current means of estimating the heading of planetary rovers involves integration of noisy rotational-speed measurements. This noise causes error to accumulate and grow rapidly. Moreover, the heading error affects the estimate of the x, y position of the rover. More importantly, incremental odometry heading estimation is only reliable over relatively short distances. There is an urgent need to develop a new heading-detection sensor for long traverses (for example, 100 m per Sol [Martian Day]), as outlined for the 2003 Mars mission. Results of a recent FIDO field trial at Black Rock Summit in Central Nevada and several Operations Readiness Test (ORTs) at the JPL MarsYard using the Sun-sensor have demonstrated three- to four-fold improvement in the heading estimation of the rover compared to incremental odometry. These test results helped shape the mission

14. SUBJECT TERMS
Planetary Rover, Sun Sensor, Heading Estimation

15. NUMBER OF PAGES
36

16. PRICE CODE

17. SECURITY CLASSIFICATION OF REPORT	18. SECURITY CLASSIFICATION OF THIS PAGE	19. SECURITY CLASSIFICATION OF ABSTRACT	20. LIMITATION OF ABSTRACT
Unclassified	Unclassified	Unclassified	UL